chemistry

MDPI

Article

The B_2 Structural Motif as a Tool for Modulating Ring Currents in Monocyclic Li Clusters

Slađana Đorđević and Slavko Radenković *

Faculty of Science, University of Kragujevac, Radoja Domanovića 12, 34000 Kragujevac, Serbia; sladjana.djordjevic@pmf.kg.ac.rs

* Correspondence: slavkoradenkovic@kg.ac.rs

Abstract: Magnetically induced current densities, calculated at the M06-2X/def2-TZVP level using the diamagnetic-zero version of the continuous transformation of origin of current density (CTOCD-DZ) method, were employed to study the aromaticity in $Li_3B_2^-$ and Li_4B_2. It was found that the Li_3/Li_4 rings in $Li_3B_2^-$ and Li_4B_2 remarkably resemble the monocyclic Li_3^+ and Li_4^{2+} clusters. Unlike the parent Li_3^+ and Li_4^{2+} systems that sustain negligibly weak global current density circulation, the $Li_3B_2^-$ and Li_4B_2 clusters exhibit a strong diatropic current density. The present work demonstrates how structural modifications introduced by the B_2 unit can be used for modulating the current density in cyclic Li-based clusters.

Keywords: current density; aromaticity; Li clusters; ab initio calculations

Citation: Đorđević, S.; Radenković, S. The B_2 Structural Motif as a Tool for Modulating Ring Currents in Monocyclic Li Clusters. *Chemistry* **2021**, *3*, 1063–1073. https://doi.org/10.3390/chemistry3030077

Academic Editors: Andrea Peluso and Guglielmo Monaco

Received: 28 July 2021
Accepted: 4 September 2021
Published: 14 September 2021

1. Introduction

Cyclic electron delocalization is among the most intriguing phenomena in chemistry. If present in a molecule, cyclic electron delocalization determines rather unique structural, magnetic, thermodynamic, and reactivity-based properties [1–3]. All these features coming due to cyclic electron delocalization are usually referred to as aromaticity. Understanding, defining, and evaluating the magnetic aspects of molecular aromaticity have been in focus of chemists for almost a whole century [4,5]. Already, London [6] recognized that an aromatic molecule sustains an induced ring current as a response to the applied external magnetic field perpendicular to the molecular plane. Nowadays, it is widely accepted that the specific behavior of molecules in the presence of the external magnetic field can be used for qualitative and quantitative assessment of aromaticity [4,5,7,8]. The magnetically induced current density is the most important concept in the evaluation of the magnetic aspect of aromaticity. Based on the current densities, one can measure both global and local aromaticity [8]. In addition, other indices of magnetic aromaticity, including the nucleus-independent chemical shift (NICS) [9], as one of the most employed aromaticity indices, can be obtained from the induced current density [4,10]. On the other hand, there is no unique way to reconstruct current density maps from NICS values [11].

One of the most important challenges in the computation of magnetically induced current densities and related molecular magnetic response properties is how to treat the so-called gauge origin problem [8]. The gauge origin problem refers to the dependence of the calculated magnetic properties on the translation of the origin of the coordinate system. The gauge origin problem can be generally eliminated either by employing a basis set with an explicit magnetic field dependence or by an explicit treatment of the gauge origin dependence [8]. The first group of methods are based on perturbation-dependent basis functions, such as gauge-including atomic orbitals (GIAO) [6]. Calculation of the induced current density by means of the GIAO can be performed by means of the gauge-including magnetically induced current (GIMIC) method [8,12]. Within the second approach, the most employed methods are based on the continuous transformations of origin of current density (CTOCD) technique [13,14]. In this approach, the gauge origin problem is resolved

by using a different gauge origin for each point for which the current density is calculated. It should be noted that this method was originally introduced as the so-called continuous set of gauge transformation (CSGT) method and that the name CTOCD was suggested somewhat later [15–17]. Over almost a half of a century, Riccardo Zanasi contributed to the development of the CTOCD method and other approaches for calculation of the magnetic response properties, as well as in the software implementation of these theories [18,19]. In the present work, the diamagnetic zero (DZ) version of the CTOCD method was employed. In the CTOCD-DZ, also known as the *ipsocentric* method [20,21], the current density at each point is calculated by choosing itself as the origin of the vector potential. More details on the CTOCD method can be found in reviews [4,16] and elsewhere [22].

There are many cases showing that the NICS and current density results do not always agree [23–27]. One of the most-known examples is the monocyclic Li_3^+ cluster. Li_3^+ has two valence electrons, and according to the Hückel 4n + 2 rule, this system should be aromatic. Large negative NICS values wrongly predicted the aromatic character of Li_3^+ [23] because this system does not sustain global ring currents, but rather local circulations around Li atoms. In what follows, the magnetically induced current densities in two recently characterized complexes [28], $Li_3B_2^-$ and Li_4B_2, are examined and compared to those in the corresponding reference Li_3^+ and Li_4^{2+} systems. To the best of the authors' knowledge, the target $Li_3B_2^-$ and Li_4B_2 clusters have not so far been experimentally observed. However, a closely related species, $Na_3Al_2^-$, which is isoelectronic to $Li_3B_2^-$, has been recently experimentally characterized [29]. In what follows, it is shown how the presence of the B_2 unit can drastically change magnetic response properties of the parent Li_3/Li_4 ring.

2. Computational Methods

The molecular structures were fully optimized at the M06-2X/def2-TZVP level of theory by means of the Gaussian 09 program [30]. Frequency calculations confirmed that the obtained structures have no imaginary frequencies. The NBO analysis [31] was performed at the same level as implemented in Gaussian 09 program. Magnetically induced current densities were calculated at the M06-2X/def2-TZVP level using the CTOCD-DZ approach. These calculations were performed using our in-house Fortran code, which requires the data from the Gaussian 09 wfx-file (obtained with the keyword NMR = CSGT). The current densities were calculated for a grid of points belonging to the plane formed by Li atoms. The so-obtained current density maps were visualized using the Paraview program [32], utilizing the following convention: counterclockwise/clockwise circulations represent diatropic/paratropic current densities. The bond current strengths were obtained through the disc-based quadrature scheme [33], which employs numerical integration, as devised by Elhay and Kautsky [34]. The integration disc perpendicularly bisects the given bond, and the disc radius is the average of the covalent radii of the two bonded atoms.

The multicenter delocalization index (MCI) [3], which quantifies electron delocalization in a given ring, can be calculated using different partition schemes [35–37]. In this work, the natural atomic orbital (NAO) density matrices obtained from NBO analysis were used to calculate the MCI. In order to eliminate the ring-size dependence of the MCI, the nth root of the original index, denoted by $MCI^{1/n}$, was employed [3]. These calculations were performed using our in-house FORTRAN program. The NICS values were calculated at the M06-2X/def2-TZVP level of theory through the gauge-including atomic orbital (GIAO) method [38,39]. The dissected canonical molecular orbital NICS (CMO-NICS) was calculated using the NBO 7.0 program [40].

3. Results and Discussion

The optimized structures of $Li_3B_2^-$ and Li_4B_2, having C_{2v} and D_{4h} symmetries, respectively, are presented in Figure 1. These structures can be described as inverse sandwich complexes, consisting of the Li_3/Li_4 ring sandwiched between two boron atoms. Both studied complexes are characterized by a short B−B distance: 1.53 and 1.52 Å in $Li_3B_2^-$

and Li_4B_2, respectively. These B−B distances are shorter than those reported in the $Al_3B_2^-$ cluster, for which the respective B−B bond was characterized as triple [41]. It is worth noting that, according to the NBO analysis, the B−B bond in studied clusters is a triple bond: 1σ + 2π bonds.

(**a**) (**b**)

Figure 1. Optimized structures of $Li_3B_2^-$ (**a**) and Li_4B_2 (**b**) obtained at the M06-2X/def2-TZVP level of theory.

It has previously been shown that the Li_3^+ cluster exhibits the D_{3h} structure. It was found that the presence of the B_2 unit in $Li_3B_2^-$ elongates the Li−Li distances (being equal to 3.30 and 3.65 Å) with respect to that in monocyclic Li_3^+ cluster (3.05 Å) optimized at the same level of theory. The analogous planar D_{4h} geometry of the bare Li_4^{2+} complex does not correspond to minima on the potential energy surfaces. The global minimum of Li_4^{2+} was found to have tetrahedral T_d structure [42]. The strain in the Li_4 ring of the Li_4B_2 complex is reduced in comparison to the Li_3 ring in $Li_3B_2^-$. Along these lines, it was observed that Li−Li distance in Li_4B_2 is 2.89 Å, which is significantly shorter than that in $Li_3B_2^-$.

Natural atomic charges of the studied systems are shown in Figure 2. As can be seen, B atoms in $Li_3B_2^-$ and Li_4B_2 carry negative charges of −1.18 and −1.27, respectively. This reveals a significant charge transfer from Li atoms to the central B_2 unit. The obtained charges on B atoms are approximately equal to −1, and $Li_3B_2^-$ and Li_4B_2 can be viewed as charge-transfer complexes: $[B]^-[Li_3]^+[B]^-$ and $[B]^-[Li_4]^{2+}[B]^-$. The calculated dissociation energies (Table 1) showed a strong stabilizing electrostatic interaction between the Li_3^+/Li_4^{2+} and B_2^{2-} fragments in the studied clusters.

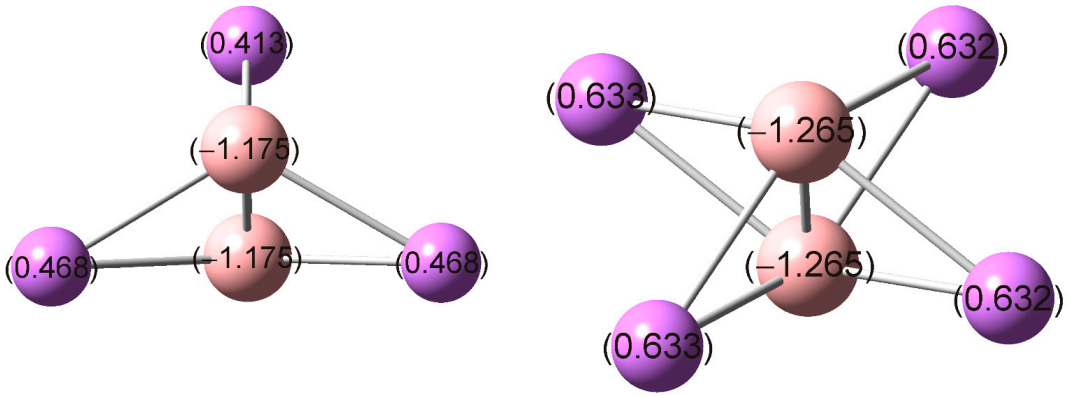

(**a**) (**b**)

Figure 2. Natural atomic charges of $Li_3B_2^-$(**a**) and Li_4B_2 (**b**) based on the natural bond orbital (NBO) analysis at the M06-2X/def2-TZVP level.

Table 1. Dissociation energies (DE, in kcal/mol) at the M06-2X/def2-TZVP level of theory.

Dissociation Path	DE
$Li_3B_2^- \rightarrow Li_3^+ + B_2^{2-}$	343.24
$Li_4B_2 \rightarrow Li_4^{2+} + B_2^{2-}$	569.61
$Li_3B_2^- \rightarrow Li_3 + B + B^-$	233.26
$Li_4B_2 \rightarrow Li_4^+ + B + B^-$	358.96
$B_2^{2-} \rightarrow 2B^-$	−18.92

The obtained structural and electronic features of $Li_3B_2^-$ indicate that the Li_3 ring in this complex bears a significant resemblance to the monocyclic Li_3^+ cluster. In what follows, the nature of magnetically induced current densities in the $Li_3B_2^-$ complex is compared with that in the monocyclic Li_3^+ cluster. As mentioned above, the global minimum of Li_4^{2+} has a tetrahedral structure. Therefore, the current density induced in Li_4B_2 will be contrasted with the monocyclic Li_4^{2+} cluster whose structure was extracted from the optimized geometry of the Li_4B_2 complex.

The calculated NICS and $MCI^{1/n}$ values of the studied systems are presented in Table 2. In order to verify these values, the diffuse functions were introduced through the ma-def2-TZVP basis set. It was revealed that the addition of the diffuse functions invokes only negligible changes in the aromaticity index values. The reference Li_3^+ and Li_4^{2+} systems are characterized by large and negative $NICS(0)_{ZZ}$ values, in agreement with the previous work [23]. The CMO σ-$NICS(0)_{ZZ}$ showed the $NICS(0)_{ZZ}$ values in these two systems are practically fully determined by the HOMO level contribution. It should be noted that the NICS(0) in $Li_3B_2^-$ and Li_4B_2 is calculated in, or very close, to the B–B bond critical point [43]. Therefore, the $NICS(0)_{ZZ}$ values cannot be used to compare the aromaticity of the target complexes and their reference Li_3^+/Li_4^{2+} systems. The $MCI^{1/n}$ values predict a high extent of electron delocalization in the reference Li_3^+ and Li_4^{2+} systems. Based on the $MCI^{1/n}$ values, the introduction of the B_2 fragment into the Li_3/Li_4 rings causes a reduction in the intensity of cyclic electron delocalization. This result goes in line with the calculated NBO-based Wiberg bond indices, which also suggest notably weaker Li–Li bonding interactions in $Li_3B_2^-$ and Li_4B_2 than in the reference bare Li-clusters.

Table 2. $MCI^{1/n}$, $NICS(0)_{ZZ}$, and CMO-$NICS(0)_{ZZ}$ values of the Li-atom rings in the studied systems. The results obtained with the ma-def2-TZVP basis set are given in the brackets.

Molecule	$MCI^{1/n}$	$NICS(0)_{ZZ}$	σ-$NICS(0)_{ZZ}$	π-$NICS(0)_{ZZ}$
$Li_3B_2^-$	0.4214 (0.4012)	−54.62 (−53.58)	−45.48	−6.2
Li_4B_2	0.3176 (0.3081)	−46.21 (−46.50)	−36.17	−6.64
Li_3^+	0.7631 (0.7631)	−9.00 (−9.06)	−11.47	-
Li_4^{2+}	0.6575 (0.6575)	−9.59 (−9.73)	−11.08	-

Current density maps of the studied $Li_3B_2^-$ and Li_4B_2 complexes, as well as those of the reference Li_3^+ and Li_4^{2+} systems, are shown in Figures 3 and 4. In agreement with the previous study [23], it can be seen that the Li_3^+ cluster shows no significant ring currents, but only local circulations around Li atoms. The same was found for the Li_4^{2+} structure (Figure 4b). On the other hand, the $Li_3B_2^-$ and Li_4B_2 systems sustain rather strong diatropic ring currents. The most striking feature of the ring currents in $Li_3B_2^-/Li_4B_2$ is that the strongest circulations occur inside the Li_3/Li_4 rings and around the B–B bonds. The obtained current densities in $Li_3B_2^-/Li_4B_2$ resembles the current densities of π-electrons in the isolated B_2^{2-}. However, the current density maps from Figures 3 and 4 clearly show that the Li atoms are substantially involved in the circulation occurring in the ring center. In addition, the isolated B_2^{2-} unit was found to be unstable relative to the dissociation product $2B^-$ (Table 1), which also confirms a strong stabilization of the B_2^{2-} fragment thorough the interaction with Li atoms in $Li_3B_2^-$ and Li_4B_2. The obtained current densities completely oppose the conclusions derived from the MCI values.

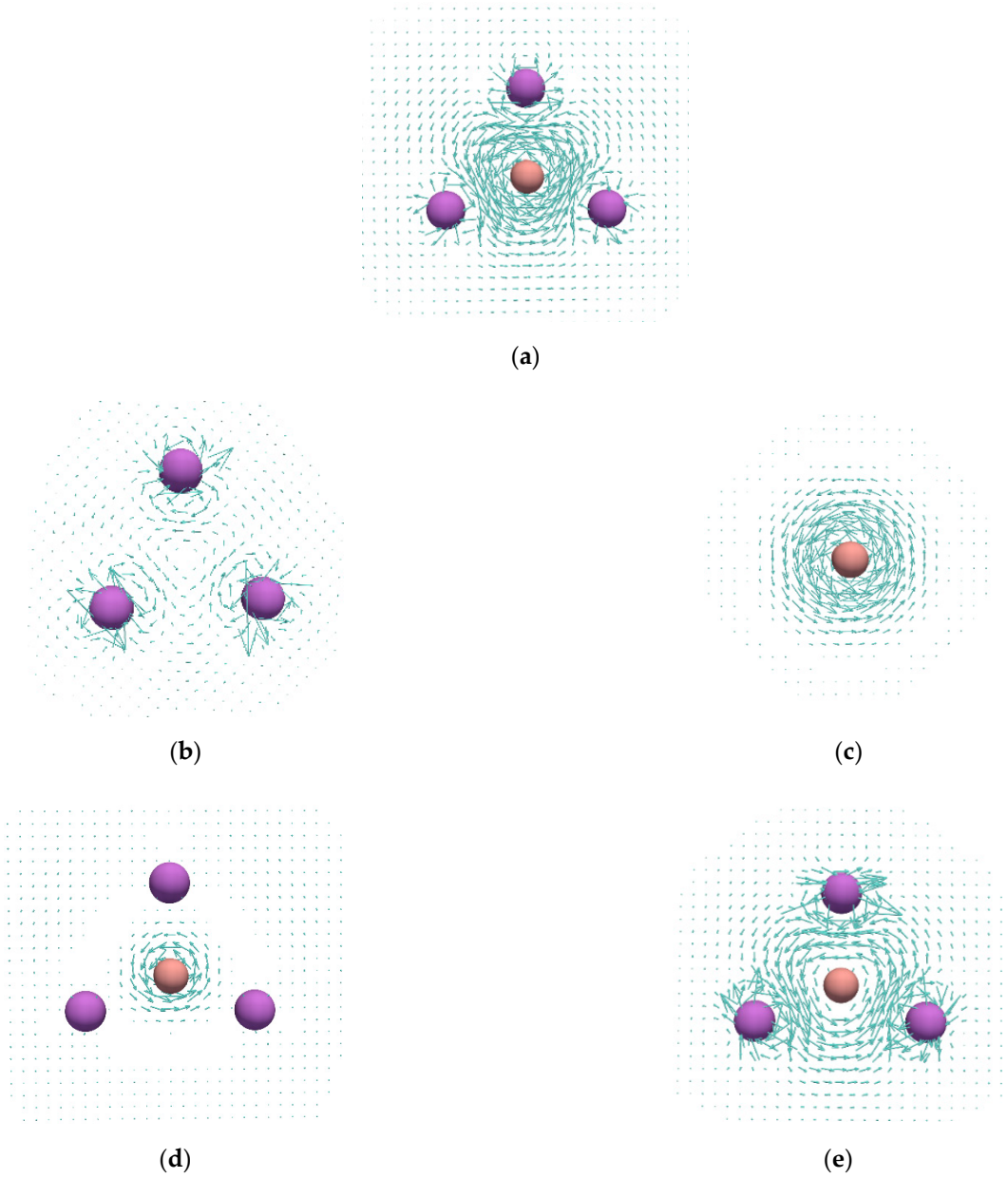

Figure 3. Current density maps calculated in the plane of the Li-atom ring: $Li_3B_2^-$ (**a**), Li_3^+ (**b**), HOMO of $Li_3B_2^-$ (**d**), quasi-doubly degenerate HOMO-1 of $Li_3B_2^-$ (**e**); current densities plotted in the plane that perpendicularly bisects the B–B bond of the B_2^{2-} fragment extracted from the optimized geometry of $Li_3B_2^-$ (**c**).

The nature of the current densities induced in the studied complexes was further analyzed by examining structures in which the B–B distances were simultaneously elongated by Δd value, while the Li-nuclei positions were kept frozen. The current density maps of the so-obtained geometries are displayed in Figure 5. As can be seen in $Li_3B_2^-$ and Li_4B_2, increasing the B–B distances leads to a continuous weakening of the current density induced inside the Li-atom rings. Table 3 contains natural atomic charges of B atoms, as well as aromaticity indices of Li-atom rings obtained for the structures with the modified B–B distances. As can be seen, the charge of B atoms changes from around -1, at the equilibrium distance, to approximately $-1/2$ at the dissociation limit. In other words, the B_2 unit changes the charge from -2 to -1. While the $NICS(0)_{ZZ}$ values show the same trend as the current densities and NBO charges, the $MCI^{1/n}$ magnitudes do not change regularly with increasing distance between B atoms in the studied complexes. The $MCI^{1/n}$ also confirms that the B–B bond elongation reduces the intensity of cyclic delocalization

in the two clusters. This implies that both $MCI^{1/n}$ and current density give the same prediction on the aromatic character of the Li_3/Li_4^+ systems obtained by the B–B bond elongation in the examined $Li_3B_2^-$ and Li_4B_2 clusters. The energetic data from Table 1 show that the dissociation of the studied complexes in Li_3/Li_4^+ and B_2^- fragments is thermodynamically preferred over the dissociation in Li_3^+/Li_4^{2+} and B_2^{2-} fragments.

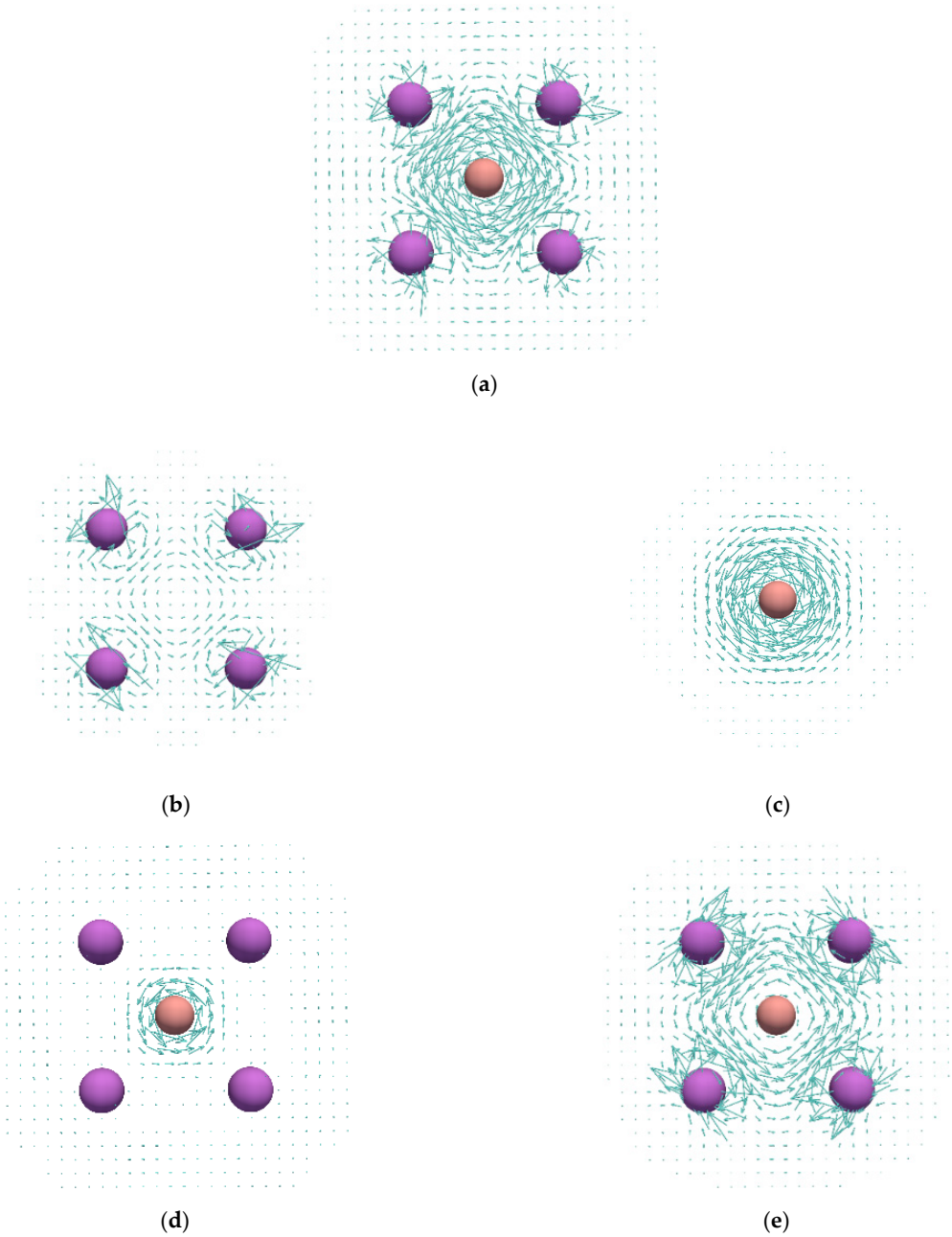

Figure 4. Current density maps calculated in the plane of the Li-atom ring: Li_4B_2 (**a**), Li_4^{2+} (**b**), HOMO of Li_4B_2 (**d**), doubly degenerate HOMO-1 of Li_4B_2 (**e**); current densities plotted in the plane that perpendicularly bisects the B–B bond of the B_2^{2-} fragment extracted from the optimized geometry of Li_4B_2 (**c**).

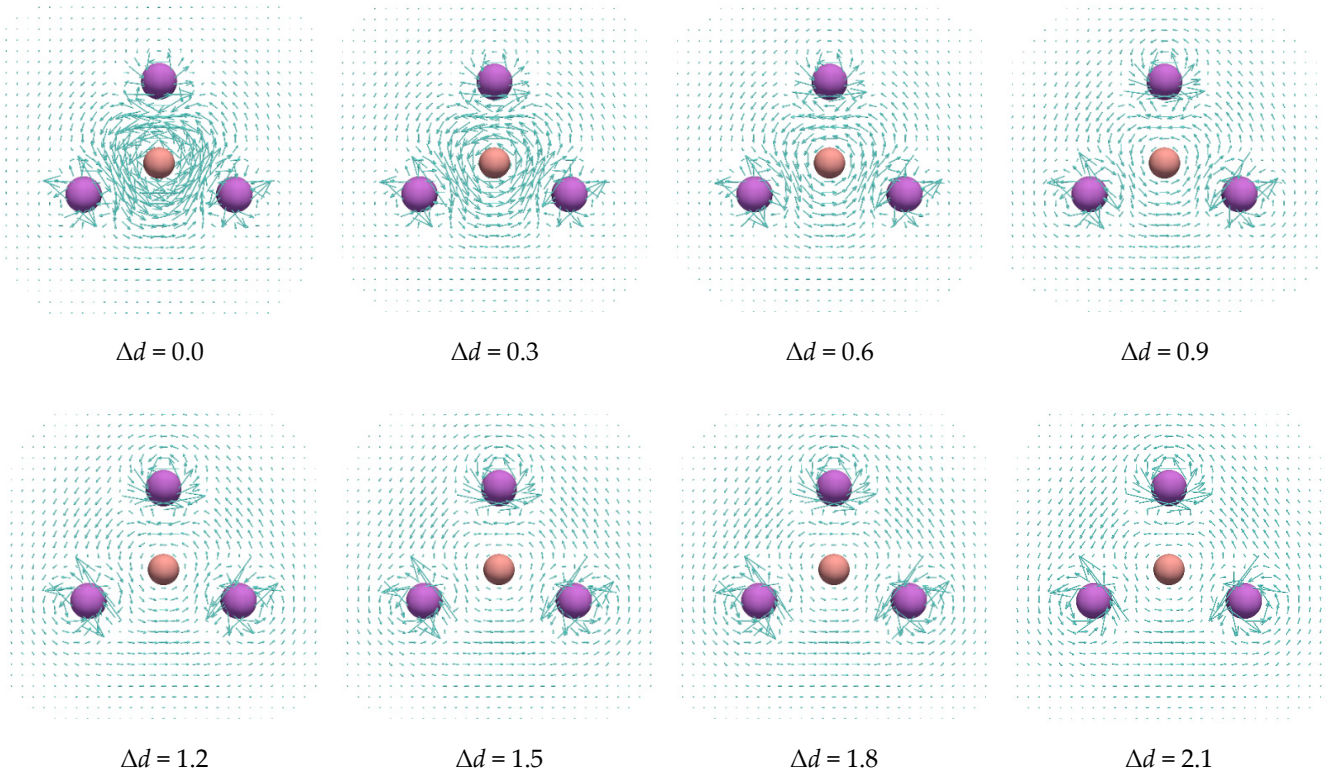

Figure 5. Current density maps of the structures in which, starting from the optimized geometries of $Li_3B_2^-$ (**a**) and Li_4B_2 (**b**), the B–B distances were elongated by Δ*d* (in Å), while the Li-atom positions were kept unchanged.

Table 3. Natural atomic charges of B atoms, $NICS(0)_{ZZ}$, and $MCI^{1/n}$ values of the structures in which the B–B distances were simultaneously elongated by Δd value, while the Li-nuclei positions were kept unchanged.

Δd	Charge of B		$NICS(0)_{ZZ}$		$MCI^{1/n}$	
	$Li_3B_2^-$	Li_4B_2	$Li_3B_2^-$	Li_4B_2	$Li_3B_2^-$	Li_4B_2
0.0	−1.175	−1.265	−54.62	−46.21	0.4213	0.3178
0.3	−1.179	−1.265	−49.89	−46.03	0.2581	0.3146
0.6	−1.161	−1.148	−40.86	−36.03	0.1613	0.1495
0.9	−1.089	−0.947	−31.87	−28.46	0.2728	0.2141
1.2	−0.886	−0.717	−25.67	−24.02	0.2571	0.1968
1.5	−0.740	−0.551	−22.21	−22.17	0.2444	0.1821
1.8	−0.621	−0.414	−20.16	−21.45	0.2315	0.1899
2.1	−0.513	−0.293	−19.01	−21.55	0.2237	0.2258

Current density maps are mainly used as a qualitative tool, and for quantitative purposes, the bond current strengths can be utilized. Table 4 presents bond current strengths for the studied molecules. The $Li_3B_2^-$ and Li_4B_2 complexes sustain strong diatropic current densities, with the respective bond current strengths of 8.81/8.57 and 8.11 nA T^{-1}. For comparison, the C–C bond current strength for benzene at the same level of theory is 4.75 nA T^{-1}. The obtained results show that the magnetic properties of the Li_3^+/Li_4^{2+} systems are substantially modulated with the introduction of the B_2^{2-} unit.

Table 4. Bond current strengths (in nA T^{-1}) for all symmetry-unique bonds.

Bond	Li_3^+	Li_4^{2+}	$Li_3B_2^-$	Li_4B_2
Li1–Li2	2.28	1.59	8.81	8.11
Li2–Li3			8.57	

Within the ipsocentric method, total current density can be partitioned into molecular orbital contributions. The HOMO electrons in $Li_3B_2^-$ and Li_4B_2 contribute to a rather weak circulation that occurs in the very center of the Li_3/Li_4 ring (Figures 3d and 4d). On the other hand, the quasi-degenerate HOMO-1 $(2b_1+5a_1)$ level in $Li_3B_2^-$ and the doubly degenerate HOMO-1 $(2e_u)$ level in Li_4B_2 give the most important contribution to the total current density (Figures 3e and 4e).

Relevant subsections of the orbital interaction diagrams of the Li_3^+/Li_4^{2+} and B_2^{2-} fragment valence orbitals are shown in Figures 6 and 7. The HOMO $(6a_1)$ in $Li_3B_2^-$ is formed by mixing HOMO of Li_3^+ and LUMO of the B_2^{2-} fragment. The quasi-degenerate HOMO-1 level, consisting of $2b_1$ and $5a_1$ orbitals, comes as a result of the combination of LUMO of the Li_3^+ fragment and the degenerate HOMO-1 level of the B_2^{2-} fragment. The same bonding situation was found in Li_4B_2 (Figure 7).

The CTOCD-DZ approach provides a unique interpretative capability, as the orbital current density contributions can be related to the virtual transitions between occupied and virtual orbitals. The virtual transitions must obey symmetry-based selection rules [20,21]. If the product of symmetries of the occupied and virtual orbitals contains the in-plane translation/rotation, then the given virtual excitation contributes to diatropic/paratropic current density. As already shown [23], the HOMO current density rather weakly contributes to the global currents in Li_3^+ because the effect of the translational transition from HOMO $(2a_1')$ to LUMO $(2e')$ is annulled by the rotational transition to the virtual orbital $1a_2'$ (Figure 6). In $Li_3B_2^-$, the HOMO electrons give small contribution to the global circulation. This is because the translational transition from HOMO $(6a_1)$ to LUMO $(3b_1)$ is accompanied by the rotational transition to the $5b_1$ orbital. There are translational transitions from the quasi-doubly degenerate HOMO-1 $(2b_1+5a_1)$ level to the quasi-doubly degenerate virtual orbital level $4b_1+9a_1$. These transitions are of the most importance for the global circulation in the $Li_3B_2^-$ cluster.

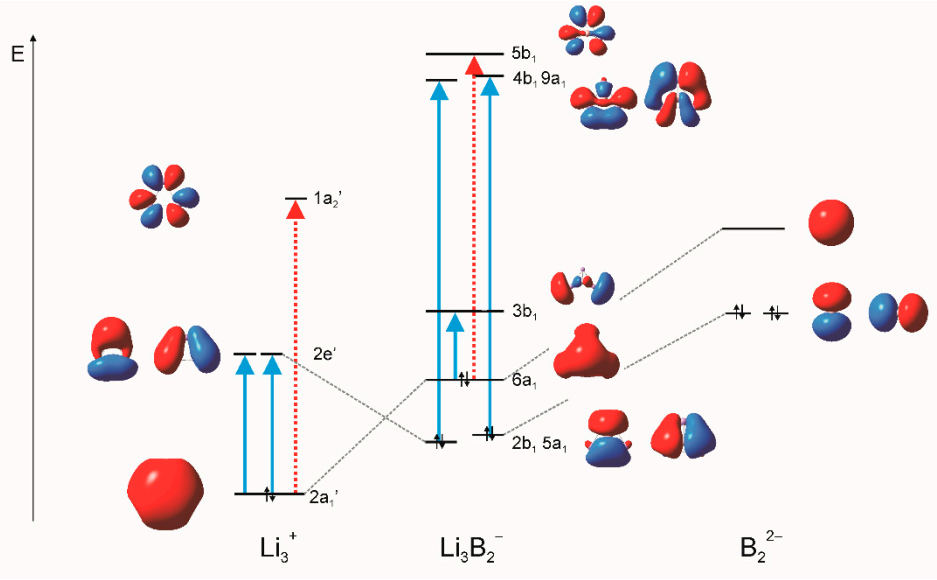

Figure 6. Orbital interaction diagram of $Li_3B_2^-$ obtained at the M06-2X/def2-TZVP level of theory. Full (blue) arrows represent the main translational transitions, and dashed (red) arrows represent the main rotational transitions.

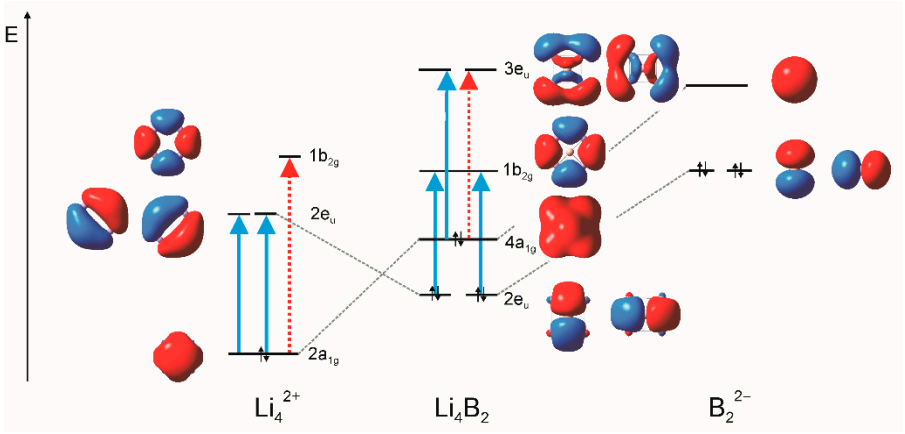

Figure 7. Orbital interaction diagram of Li_4B_2 obtained at the M06-2X/def2-TZVP level of theory. Full (blue) arrows represent the main translational transitions, and dashed (red) arrows represent the main rotational transitions.

A very similar relation between the found magnetic properties and electronic structure can be found in the Li_4B_2 system. Figure 7 demonstrates that the HOMO electrons in Li_4^{2+} induce weak currents because of the two supposed transitions: translational and rotational from HOMO $(4a_{1g})$ to LUMO $(3e_u)$. This way, the HOMO current density contribution is quite small. On the other hand, the translational transition from the doubly degenerate HOMO-1 $(2e_u)$ level to the virtual $1b_{2g}$ level gives rise to the strong currents induced by the HOMO-1 electrons.

4. Conclusions

The present paper shows how the B_2 unit can be used for the rational structural modifications of cyclic Li-based clusters, which can cause substantial changes in their aromatic characteristics. The magnetically induced current densities, as the most reliable magnetic criterion, revealed the aromatic character of $Li_3B_2^-$ and Li_4B_2 clusters. The orbital analysis showed that in both $Li_3B_2^-$ and Li_4B_2, the main contribution to the global currents comes from the doubly degenerate HOMO-1 level, which can be deduced from the

combination of the LUMO of the Li_3^+/Li_4^{2+} fragment and the doubly degenerate π-MO level of the B_2^{2-} fragment. Quite surprisingly, the MCI values predict a low level of electron delocalization in $Li_3B_2^-$ and Li_4B_2 clusters and, on the other hand, intensive electron delocalization in the reference Li_3^+/Li_4^{2+} systems. It is difficult to understand such a difference between the current-density- and electron-delocalization-based aromaticity predictions, and its rationalization will remain a task for the future.

Author Contributions: Conceptualization, S.R.; methodology, S.R.; software, S.R.; investigation, S.Đ.; writing—original draft preparation, S.Đ.; writing—review and editing, S.R.; visualization, S.Đ. Both authors have read and agreed to the published version of the manuscript.

Funding: This work was supported by the Serbian Ministry of Education, Science and Technological Development (Agreement No. 451-03-68/2020-14/200122).

Data Availability Statement: The data presented in this study are available on request from the corresponding author.

Acknowledgments: The authors would like to thank Dušan Ćoćić and Ralph Puchta for helping us in calculations of CMO-NICS indices. We would like to thank Tim Clark and Wolfgang Hieringer for hosting these calculations at the CCC. The authors gratefully acknowledge the Regionales Rechenzentrum Erlangen (RRZE) for a generous allotment of computer time.

Conflicts of Interest: The authors declare no conflict of interest.

References

1. Cyrański, M.K. Energetic Aspects of Cyclic π-Electron Delocalization: Evaluation of the Methods of Estimating Aromatic Stabilization Energies. *Chem. Rev.* **2005**, *105*, 3773–3811. [CrossRef] [PubMed]
2. Gershoni-Poranne, R.; Stanger, A. Magnetic Criteria of Aromaticity. *Chem. Soc. Rev.* **2015**, *44*, 6597–6615. [CrossRef] [PubMed]
3. Feixas, F.; Matito, E.; Poater, J.; Solà, M. Quantifying Aromaticity with Electron Delocalisation Measures. *Chem. Soc. Rev.* **2015**, *44*, 6434–6451. [CrossRef] [PubMed]
4. Lazzeretti, P. Ring Currents. *Prog. Nucl. Magn. Reson. Spectrosc.* **2000**, *36*, 1–88. [CrossRef]
5. Gomes, J.A.N.F.; Mallion, R.B. Aromaticity and Ring Currents. *Chem. Rev.* **2001**, *101*, 1349–1384. [CrossRef] [PubMed]
6. London, F. Théorie Quantique des Courants Interatomiques dans les Combinaisons Aromatiques. *J. Phys. Radium* **1937**, *8*, 397–409. [CrossRef]
7. Geuenich, D.; Hess, K.; Köhler, F.; Herges, R. Anisotropy of the Induced Current Density (ACID), a General Method to Quantify and Visualize Electronic Delocalization. *Chem. Rev.* **2005**, *105*, 3758–3772. [CrossRef]
8. Sundholm, D.; Fliegl, H.; Berger, R.J.F. Calculations of Magnetically Induced Current Densities: Theory and Applications. *Wiley Interdiscip. Rev. Comput. Mol. Sci.* **2016**, *6*, 639–678. [CrossRef]
9. Schleyer, P.v.R.; Maerker, C.; Dransfeld, A.; Jiao, H.; Hommes, N.J.v.R.E. Nucleus-Independent Chemical Shifts: A Simple and Efficient Aromaticity Probe. *J. Am. Chem. Soc.* **1996**, *118*, 6317–6318. [CrossRef]
10. Lazzeretti, P. Assessment of Aromaticity via Molecular Response Properties. *Phys. Chem. Chem. Phys.* **2004**, *6*, 217–223. [CrossRef]
11. Van Damme, S.; Acke, G.; Havenith, R.W.A.; Bultinck, P. Can the Current Density Map Topology Be Extracted from the Nucleus Independent Chemical Shifts? *Phys. Chem. Chem. Phys.* **2016**, *18*, 11746–11755. [CrossRef]
12. Jusélius, J.; Sundholm, D.; Gauss, J. Calculation of Current Densities Using Gauge-Including Atomic Orbitals. *J. Chem. Phys.* **2004**, *121*, 3952–3963. [CrossRef]
13. Keith, T.A.; Bader, R.F.W. Calculation of Magnetic Response Properties Using a Continuous Set of Gauge Transformations. *Chem. Phys. Lett.* **1993**, *210*, 223–231. [CrossRef]
14. Keith, T.A.; Bader, R.F.W. Topological Analysis of Magnetically Induced Molecular Current Distributions. *J. Chem. Phys.* **1993**, *99*, 3669–3682. [CrossRef]
15. Lazzeretti, P.; Malagoli, M.; Zanasi, R. Computational Approach to Molecular Magnetic Properties by Continuous Transformation of the Origin of the Current Density. *Chem. Phys. Lett.* **1994**, *220*, 299–304. [CrossRef]
16. Lazzeretti, P. Methods of Continuous Translation of the Origin of the Current Density Revisited. *Theor. Chem. Acc.* **2012**, *131*, 1222. [CrossRef]
17. Zanasi, R. Coupled Hartree-Fock Calculations of Molecular Magnetic Properties Annihilating the Transverse Paramagnetic Current Density. *J. Chem. Phys.* **1996**, *105*, 1460–1469. [CrossRef]
18. Lazzeretti, P.; Zanasi, R. *SYSMO Package*; University of Modena: Modena, Italy, 1980.
19. Monaco, G.; Summa, F.F.; Zanasi, R. Program Package for the Calculation of Origin-Independent Electron Current Density and Derived Magnetic Properties in Molecular Systems. *J. Chem. Inf. Model.* **2021**, *61*, 270–283. [CrossRef]
20. Steiner, E.; Fowler, P.W. Patterns of Ring Currents in Conjugated Molecules: A Few-Electron Model Based on Orbital Contributions. *J. Phys. Chem. A* **2001**, *105*, 9553–9562. [CrossRef]

21. Steiner, E.; Fowler, P.W. Four- and Two-Electron Rules for Diatropic and Paratropic Ring Currents in Monocyclic π Systems. *Chem. Commun.* **2001**, 2220–2221. [CrossRef]
22. Soncini, A.; Teale, A.M.; Helgaker, T.; De Proft, F.; Tozer, D.J. Maps of Current Density Using Density-Functional Methods. *J. Chem. Phys.* **2008**, *129*, 74101. [CrossRef] [PubMed]
23. Havenith, R.W.A.; De Proft, F.; Fowler, P.W.; Geerlings, P. σ-Aromaticity in H_3^+ and Li_3^+: Insights from Ring-Current Maps. *Chem. Phys. Lett.* **2005**, *407*, 391–396. [CrossRef]
24. Badri, Z.; Pathak, S.; Fliegl, H.; Rashidi-Ranjbar, P.; Bast, R.; Marek, R.; Foroutan-Nejad, C.; Ruud, K. All-Metal Aromaticity: Revisiting the Ring Current Model among Transition Metal Clusters. *J. Chem. Theory Comput.* **2013**, *9*, 4789–4796. [CrossRef] [PubMed]
25. Foroutan-Nejad, C. Is NICS a Reliable Aromaticity Index for Transition Metal Clusters? *Theor. Chem. Acc.* **2015**, *134*, 1–9. [CrossRef]
26. Foroutan-Nejad, C.; Vícha, J.; Ghosh, A. Relativity or Aromaticity? A First-Principles Perspective of Chemical Shifts in Osmabenzene and Osmapentalene Derivatives. *Phys. Chem. Chem. Phys.* **2020**, *22*, 10863–10869. [CrossRef] [PubMed]
27. Radenković, S.; Bultinck, P. Ring Currents in Polycyclic Sodium Clusters. *J. Phys. Chem. A* **2011**, *115*, 12493–12502. [CrossRef]
28. Kalita, A.; Rohman, S.; Kashyap, C.; Ullah, S.; Baruah, I.; Marumder, L.; Das, K.; Guha, A. Boron-Boron Quadruple Bond in $Li_3B_2^-$ and Li_4B_2 Clusters. *Phys. Chem. Chem. Phys.* **2021**. [CrossRef]
29. Zhang, X.; Popov, I.A.; Lundell, K.A.; Wang, H.; Mu, C.; Wang, W.; Schnöckel, H.; Boldyrev, A.I.; Bowen, K.H. Realization of an Al≡Al Triple Bond in the Gas-Phase $Na_3Al_2^-$ Cluster via Double Electronic Transmutation. *Angew. Chem. Int. Ed.* **2018**, *57*, 14060–14064. [CrossRef]
30. Frisch, M.J.; Trucks, G.W.; Schlegel, H.B.; Scuseria, G.E.; Robb, M.A.; Cheeseman, J.R.; Scalmani, G.; Barone, V.; Mennucci, B.; Petersson, G.A.; et al. *Gaussian 09*; Gaussian Inc.: Wallingford, CT, USA, 2009.
31. Foster, J.P.; Weinhold, F. Natural Hybrid Orbitals. *J. Am. Chem. Soc.* **1980**, *102*, 7211–7218. [CrossRef]
32. Ayachit, U. *The ParaView Guide: A Parallel Visualization Application*; Kitware: New York, NY, USA, 2015; ISBN 978-1930934306.
33. Irons, T.J.P.; Spence, L.; David, G.; Speake, B.T.; Helgaker, T.; Teale, A.M. Analyzing Magnetically Induced Currents in Molecular Systems Using Current-Density-Functional Theory. *J. Phys. Chem. A* **2020**, *124*, 1321–1333. [CrossRef]
34. Elhay, S.; Kautsky, J. Algorithm 655: IQPACK: FORTRAN Subroutines for the Weights of Interpolatory Quadratures. *ACM Trans. Math. Softw.* **1987**, *13*, 399–415. [CrossRef]
35. Bochicchio, R.; Ponec, R.; Torre, A.; Lain, L. Multicenter Bonding Within the AIM Theory. *Theor. Chem. Acc.* **2001**, *105*, 292–298. [CrossRef]
36. Heyndrickx, W.; Salvador, P.; Bultinck, P.; Solà, M.; Matito, E. Performance of 3D-Space-Based Atoms-in-Molecules Methods for Electronic Delocalization Aromaticity Indices. *J. Comput. Chem.* **2011**, *32*, 386–395. [CrossRef] [PubMed]
37. Bultinck, P.; Rafat, M.; Ponec, R.; Van Gheluwe, B.; Carbó-Dorca, R.; Popelier, P. Electron Delocalization and Aromaticity in Linear Polyacenes: Atoms in Molecules Multicenter Delocalization Index. *J. Phys. Chem. A* **2006**, *110*, 7642–7648. [CrossRef] [PubMed]
38. Wolinski, K.; Hinton, J.F.; Pulay, P. Efficient Implementation of the Gauge-Independent Atomic Orbital Method for NMR Chemical Shift Calculations. *J. Am. Chem. Soc.* **1990**, *112*, 8251–8260. [CrossRef]
39. Cheeseman, J.R.; Trucks, G.W.; Keith, T.A.; Frisch, M.J. A Comparison of Models for Calculating Nuclear Magnetic Resonance Shielding Tensors. *J. Chem. Phys.* **1996**, *104*, 5497–5509. [CrossRef]
40. Glendening, E.D.; Landis, C.R.; Weinhold, F. NBO 7.0: New Vistas in Localized and Delocalized Cbonding Theory. *J. Comput. Chem.* **2019**, *40*, 2234–2241. [CrossRef]
41. Ghorai, S.; Jemmis, E.D. A DFT Study on the Stabilization of the B≡B Triple Bond in a Metallaborocycle: Contrasting Electronic Structures of Boron and Carbon Analogues. *Chem.–A Eur. J.* **2017**, *23*, 9746–9751. [CrossRef]
42. Alexandrova, A.; Boldyrev, A. σ-Aromaticity and σ-Antiaromaticity in Alkali Metal and Alkaline Earth Metal Small Clusters. *J. Phys. Chem. A* **2003**, *107*, 554–560. [CrossRef]
43. Bader, R.F.W. Atoms in Molecules. *Acc. Chem. Res.* **1985**, *18*, 9–15. [CrossRef]